Simplify your imaging workflows

Make research imaging workflows accessible, traceable, and secure with Athena Software for Core Imaging Facilities.

Thermo Scientific™ Athena Software is a premium imaging data management platform designed for core imaging facilities that support materials science research.

Athena Software ensures traceability of images, metadata, and experimental workflows through an intuitive and collaborative web interface.

Find out more at **thermofisher.com/athena**

ThermoFisher SCIENTIFIC

ADVANCED OPTICAL MATERIALS
www.advopticalmat.de

Tunable Bulk Polymer Planar Bragg Gratings Electrified via Femtosecond Laser Reductive Sintering of CuO Nanoparticles

Stefan Kefer, Kay Bischoff, Gian-Luca Roth, Julian Haubner, Bernhard Schmauss, and Ralf Hellmann*

This contribution demonstrates and discusses electrically tunable polymer planar Bragg gratings based on bulk cyclic olefin copolymers. A lithographic single-writing-step method and femtosecond laser reductive sintering of copper(II) oxide nanoparticles are subsequently employed in order to generate buried photonic structures and copper conducting paths on top of the polymer substrate. This way, the necessary number of process steps for fabricating a planar polymer-based electro-optical device is greatly reduced. The response of a fully electrified grating structure follows temperature changes, induced by the copper conducting path, with sensitivities up to –31 pm K^{-1}. Dilatometric measurements show that the specimen's behavior is correlated to the situationally reduced thermal expansion of the bulk polymer substrate. In consequence, the tuning response of the photonic platform follows a second order polynomial, whereas a direct current of 30 mA, which correlates to a power consumption of 18.3 mW, leads to a local temperature increase and a residual Bragg wavelength shift of 19.6 K and –547 pm, respectively. Moreover, the outstanding flexibility of the proposed fabrication concept is underlined by demonstrating alternative conducting path geometries, whereas one of the additional designs is adapted to control the spectral width of the Bragg grating's reflection peak.

1. Introduction

The strive toward sophisticated fabrication technologies for thermo-optic systems is of great interest for a multitude of scientific communities, including telecommunication as well as laser and sensor technology.[1] Principally, these devices are based on integrated micro-optic elements while the additional electrical component serves the purpose of manipulating or modulating the optical signals. Based on the rapid development of integrated photonics, a multitude of thermo-optic devices has been demonstrated within the last two decades, whereas current research increasingly focuses on polymer substrates.[2] Besides exhibiting promising properties for microsystems and outstanding machinability, polymers additionally offer low-cost and environment-friendly fabrication in comparison to classical materials like silica or semiconductors.[3–5] Furthermore, they generally exhibit outstandingly large thermo-optic coefficients in combination with vastly reduced thermal conductivities.[6,7] This fact enables the generation of highly efficient tunable optical devices by equipping the polymer platform with electrodes acting as micro heater. This way, several polymer-based micro-optic devices, such as tunable filters, attenuators, switches, phase retarders, and modulators were realized.[8–14] Additionally, wavelength tunable laser systems, based on thermo-optic polymer Bragg gratings, were demonstrated.[15–18]

Up to date, all thermo-optic polymer systems are generated by employing elaborate photolithographic procedures with multiple exposure cycles, resulting in a multi-layered electrified photonic heterostructure. Normally, the device is comprised of at least four layers, buffer, core, cladding, and electrode, generated on top of a silica substrate. Alternative fabrication methods, frequently applied in combination with photolithographic steps, are various imprint or etching techniques. If the photonic device is to be equipped with a wavelength-selective Bragg grating reflector, employing these methods, or additional irradiation of the integrated waveguide by means of the phase mask technique, becomes a necessity.[19] Alternatively, it is also possible to fabricate a polymer planar Bragg grating (PPBG) within an injection-molded polymer substrate by means of a single-writing-step (SWS) procedure. This straightforward technique features the simultaneous generation of a near-surface waveguide and a Bragg grating within a bulk polymer sample. In the process, the substrate is irradiated through a stacked mask configuration, whereas the amplitude mask defines the resulting waveguide width while the grating's structural composition is correlated to the employed phase mask.[20] Besides classical optical organics like poly(methyl

S. Kefer, K. Bischoff, G.-L. Roth, J. Haubner, Prof. R. Hellmann
Applied Laser and Photonics Group
Aschaffenburg University of Applied Sciences
Wuerzburger Strasse 45, 63743 Aschaffenburg, Germany
E-mail: stefan.kefer@th-ab.de
Prof. B. Schmauss
Institute of Microwaves and Photonics
University of Erlangen-Nuremberg
Cauerstrasse 9, 91058 Erlangen, Germany
The ORCID identification number(s) for the author(s) of this article can be found under https://doi.org/10.1002/adom.202002203.

DOI: 10.1002/adom.202002203

methacrylate), the SWS technique is also compatible with novel high-grade materials, such as hybrid polymers or cyclic olefin copolymers (COC).[21,22] In the latter, PPBGs exhibiting a reflectivity up to 98% with a spectral full width at half maximum (FWHM) of 400 pm were demonstrated, whereas reflectivity and spectral width of the Bragg reflection peak as well as the waveguide's refractive index depth profile can be optimized by adapting the employed overall UV exposure.[23,24] Furthermore, COCs offer glass-transition temperatures up to 250 °C and negligible water absorption below 0.01%. This yields outstandingly robust polymer-based optical sensors capable of quantifying temperatures up to 160 °C while withstanding exceedingly harsh environmental or processing conditions.[25–28] Consequently, COC-based PPBGs unambiguously offer superb potential for thermo-optic applications.

Current research is also eagerly interested in advanced and simplified technologies for the electrification of polymer-optic platforms. Not only thermo-optic devices, but integrated electronics in general as well as micro-opto-electrical systems and biomedical lab-on-a-chip devices greatly benefit from the development of versatile and convenient fabrication methods for polymer photonic integrated circuits (PPIC). Ink-jet printing of noble-metal conducting paths is a possible solution for free-form metallization of polymers.[29] However, due to the limited availability of gold and silver and the pricing associated therewith, copper-based conductive inks have drawn a lot of interest in recent years.[30] Albeit, when employing copper as a cost-efficient alternative, the up to 350 °C annealing step, which is imperative to facilitate conductivity, limits the technique's feasibility on optical polymers.[31] Furthermore, copper structures exhibit an increased tendency toward degradation within atmospheres containing oxygen.[32] In contrast, this undesirable oxidation can be mitigated by laser reductive sintering methods. Sintering of several copper precursors, for example based on ionic solutions, copper complexes, nanoparticles (NPs), or a combination thereof, were demonstrated on various substrates, such as glasses, glass-ceramics, poly(dimethylsiloxane), and several polymers.[33–38] Using femtosecond lasers, it is additionally possible to generate complex 3D structures.[39,40] Recently, the authors were able to transfer the generation of Cu conducting paths, via femtosecond laser reductive sintering (FLRS) of copper(II) oxide NPs, on COCs, thus paving the way toward a novel fabrication method for polymer-based tunable photonic devices, such as selective wavelength reflectors or filters.[41]

This contribution demonstrates and discusses the first polymer-based spectrally tunable Bragg grating fabricated within a bulk planar COC. By combining the straightforward SWS procedure with the femtosecond laser-based electrification technique, it is possible to greatly reduce the number of necessary production steps in comparison to conventional methods. Besides examining the general thermal behavior of an electrified COC-PPBG as well as its tuning characteristics and electrical power consumption, the study also quantifies the thermal expansion behavior of injection-molded COC substrates. Additionally, the flexibility and potential of the proposed PPIC fabrication method are exemplarily shown by realizing alternative structures adapted for other purposes, such as tuning the spectral width of a PPBG's reflection signal.

2. Experimental Results

2.1. Fabrication of Tunable COC-PPBG

A thermo-optic PPBG is fabricated by combining the SWS technique with subsequent femtosecond laser-based generation of Cu conducting paths on the specimen surface, as outlined in **Figure 1**.

During the initial SWS procedure, the bulk COC, exhibiting a length of 20 mm, a width of 10 mm, and a thickness of 1.1 mm, is exposed to ultraviolet radiation generated by a krypton fluoride (KrF) excimer laser. This results in the simultaneous generation of a waveguide and a 10 mm long Bragg grating structure underneath the substrate's surface.[20] Since the photonic structures comprise an exponential refractive index depth profile and thus no distinct boundary orthogonal to the substrate surface, they can be referred to as diffused waveguides.[24,42] Subsequently, the PPBG is tempered at 130 °C for a duration of 2 h, before its upper surface is plasma treated in order to increase its hydrophilicity, an essential step for achieving a homogenous coating thickness. Afterward, the substrate is spin coated with a CuO NP solution whereas it is important that the coating procedure takes place right after plasma treatment, since the polymer's wettability decreases over time.[43,44] After drying on a hot plate for 20 min at a temperature of 80 °C, the coating exhibits a thickness of ≈30 µm, determined by means of a laser scanning microscope (VK-X210, Keyence, Neu-Isenburg, Germany). Finally, Cu conduction paths are generated by FLRS of the CuO NPs. Since the resulting electrical component is firmly attached to the polymer surface, it is possible to remove the unirradiated precursor by depositing the device in ethylene glycol.[41] However, this process step is unnecessary in the outline of fabricating a thermo-optic device and therefore omitted.

Evaluation of the COC-PPBG's reflection signal is realized by butt coupling the integrated photonic structures to a single-mode fiber (SMF). The respective Bragg peaks, before and after electrification, are also depicted in Figure 1. No impact on signal amplitude due to the applied Cu structure is observed. However, the Bragg peak experiences a blue shift $\Delta\lambda_B$ of −200 pm and a FWHM increase Δ_{FWHM} of 36 pm. Since these alterations are first observed after the final sintering step, they are either attributed to local strain fields introduced by the copper-polymer interconnection, or laser-induced microdamage at the substrate surface. The final thermo-optic COC-PPBG exhibits a Bragg wavelength of 1550 nm and a spectral FWHM of 427 pm. The appearance of one single reflection peak with a narrow spectral width either indicates single-mode behavior of the embedded waveguide or single-mode excitation due to the butt-coupling process.[45]

2.2. Setup and Thermal Referencing

Prior to examining the thermo-optic behavior of the fabricated device, the PPBG's general behavior under the influence of thermal variations is examined. This is achieved by interrogating the temperature-induced Bragg wavelength shift $\Delta\lambda_B$, which is linked to the grating's normalized effective refractive index change $\Delta n/n_{eff}$ and its thermal expansion α by

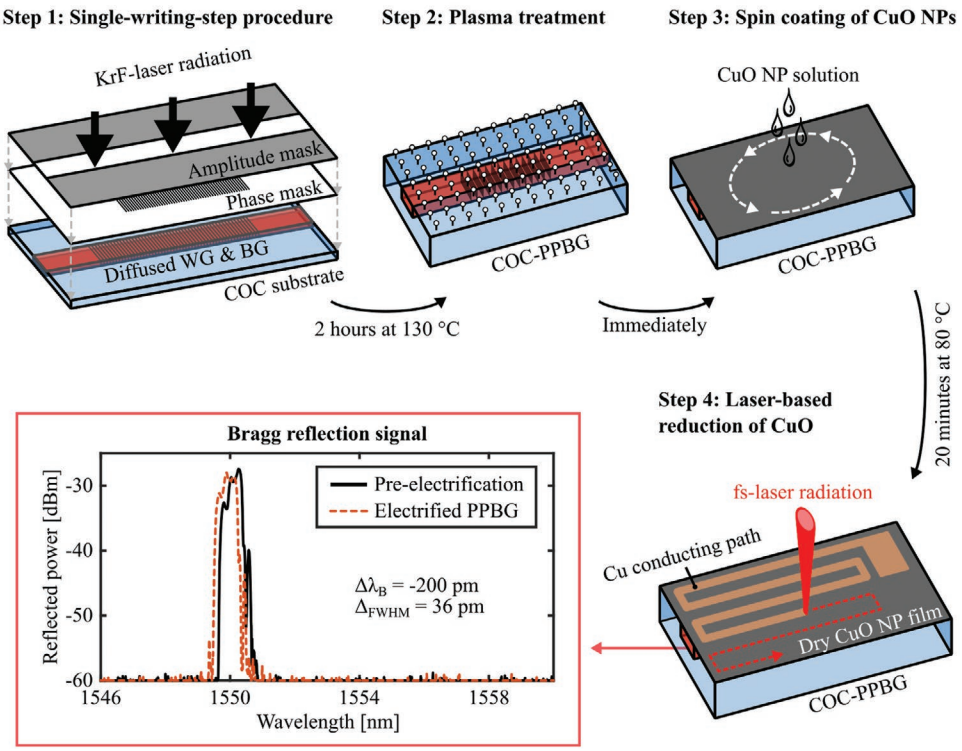

Figure 1. Fabrication procedure of thermo-optic COC-PPBGs. First, diffused waveguide and Bragg grating are generated within the polymer substrate by employing the SWS procedure. After a tempering cycle, the polymer surface is plasma treated for optimized hydrophilicity. Subsequently, the PPBG is spin-coated with a CuO-nanoparticle (NP) solution. Finally, after drying the precursor, Cu conducting paths are generated on top of the polymer by femtosecond laser reductive sintering (FLRS) of the CuO NPs. The bottom left shows the COC-PPBG's Bragg reflection signal prior and after its electrification, but with no current supply.

$$\frac{\Delta\lambda_B}{\lambda_B} = \left(\frac{\Delta n}{n_{eff}} + \alpha\right)\Delta T \tag{1}$$

Here, ΔT is the grating's absolute temperature change whereas λ_B represents its initial Bragg wavelength.[46] Simultaneously, a second SMF with orthogonally cleaved end facet is brought in close proximity with the polymer substrate's backside, whereas fiber and substrate end facet are aligned parallel to each other in order to form a Fabry–Pérot cavity. According to

$$\mathrm{FSR} = \frac{c}{2L} \tag{2}$$

wherein c represents the speed of light, the interferometer's free spectral range FSR is inversely proportional to the length L of its cavity. In this configuration, the refractive index of the air-filled cavity is assumed as 1. Thus, the change in FSR can be used for dilatometric quantification of the COC substrate's thermal expansion. The COC-PPBG is backed up against a fixed end stop to ensure that thermal expansion only takes place in direction of the Fabry–Pérot cavity. Additionally, there is sufficient horizontal offset between integrated waveguide and cavity to prevent unwanted interaction with light exiting the waveguide. A schematic as well as a photograph of the employed setup is depicted in **Figure 2**.

Figure 3, on the other hand, shows the PPBG's Bragg wavelength shift and the determined overall thermal expansion, a superposition of hotplate and polymer length variation, as a function of their temperature. Additionally, a reference measurement of only the hotplate's thermal expansion, acquired by forming a Fabry–Pérot cavity in-between hotplate and SMF, is given. This additional measurement data enables absolute quantification of the PPBG's thermal expansion by subtracting the hotplate's expansion from the determined overall expansion. According to Figure 2c, linear regression of the Bragg wavelength shift yields a thermal sensitivity of −5.1 pm K^{-1}, a value comparable to unmodified COC-PPBGs.[26]

Consequently, there is negligible impact of the electrification procedure on the PPBG's behavior when the device is exposed to environmental temperature changes. The aluminum hotplate's absolute expansion over a length of 10 cm, from its center to its outer edge, is determined as 2.36 µm K^{-1}, which yields a thermal expansion coefficient of 2.36×10^{-5} K^{-1}. This value correlates well to those given in respective literature.[47] Monitoring of the thermal expansion at the polymer backside results in an overall expansion of 3.02 µm K^{-1}. However, this value includes expansion of the hotplate over a length of 8 cm, from its center to the end stop. Subtraction of the hotplate expansion from the overall expansion results in a thermal expansion coefficient of 5.62×10^{-5} K^{-1} for the COC. This value is specified as 5.9×10^{-5} K^{-1} by the manufacturer of the virgin polymer resin.[48] Inserting the obtained data into Equation (1) yields a temperature-induced refractive index change Δn of -9.04×10^{-5} K^{-1}, a result comparable to preliminary

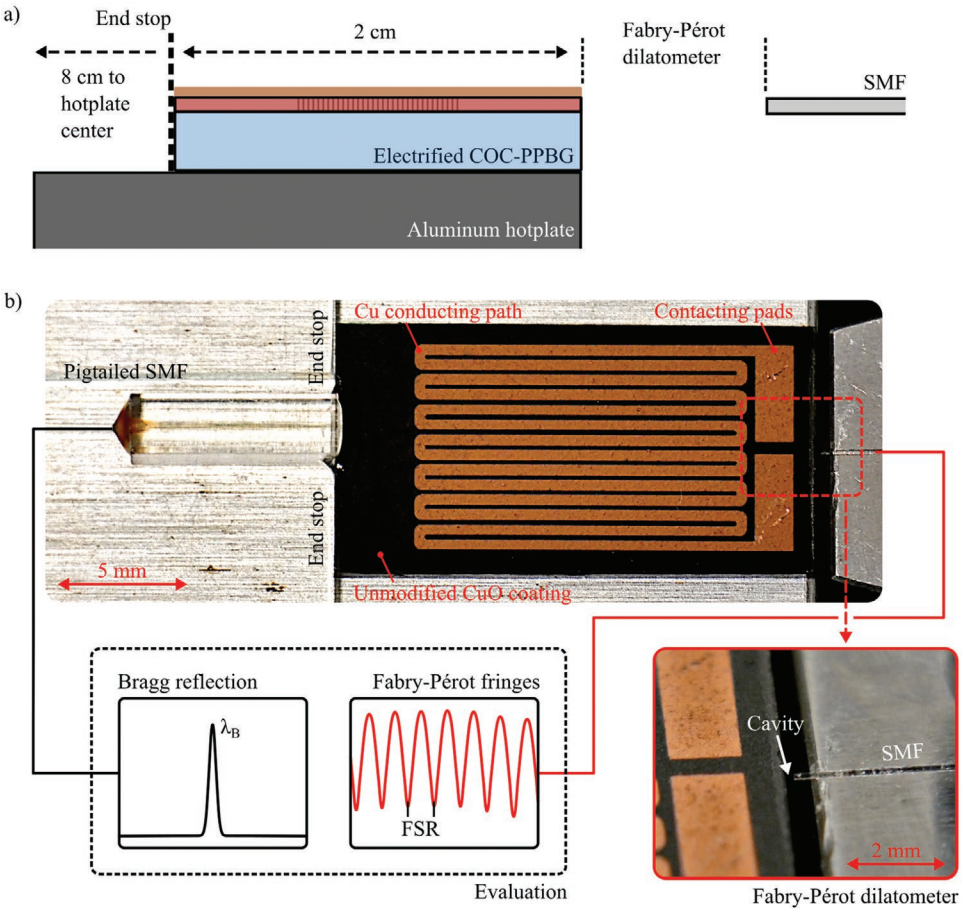

Figure 2. a) Schematic and b) image of the employed experimental setup. The COC-PPG is placed on an aluminum hotplate. Its integrated waveguide is butt coupled to a pigtailed standard single-mode fiber (SMF) in order to evaluate the Bragg reflection signal. Another SMF, exhibiting an orthogonally cleaved end facet, is brought in close proximity to the polymer substrate's backside to form a Fabry–Pérot-based dilatometer.

thermo-optic coefficient measurements of UV-modified COCs.[24] Thus, the demonstrated results and their general comparability to precedent data underline the functionality of the employed Fabry–Pérot dilatometer and that the electrification process does not interfere with the PPBG's performance or characteristics.

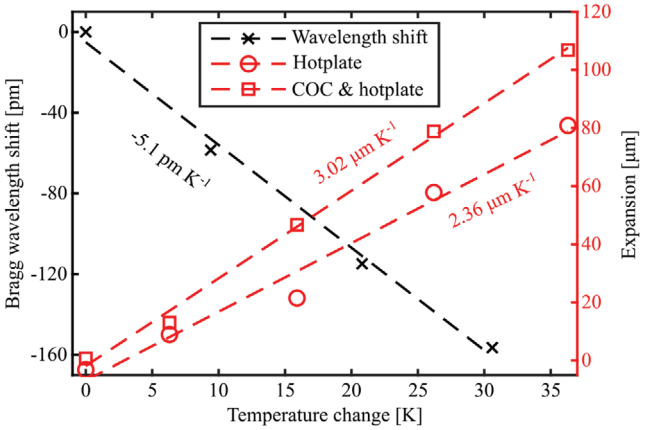

Figure 3. Resulting Bragg wavelength shift and overall expansion of the hotplate, or superimposed expansion of hotplate and COC substrate, as a function of temperature change.

2.3. Thermo-Optic Bragg Wavelength Tuning

After contacting the Cu conducting path, the PPIC is supplied with a direct current source (Digital Sourcemeter 2420, Keithley, Ohio, Solon, USA). Simultaneously, as shown in **Figure 4a**, a reference thermometer (OTG-F, Opsens, Québec, Canada) is used to determine the Cu structure's surface temperature. Due to the fact that the lateral width of a Cu conducting line is at least 17 times larger than that of the diffused photonic structures buried underneath (see Figure 4b), the actual heating element is one single Cu line. Furthermore, only the line section covering the Bragg grating is responsible for thermo-optic tuning effects.

Figure 4c exemplarily depicts the resulting Bragg wavelength shift when supplying the Cu conducting path with a current of 28 mA as well as the structure's surface temperature change. An unambiguous correlation between conduction path temperature and optical signal response can be observed, whereas the Bragg wavelength perfectly follows the determined

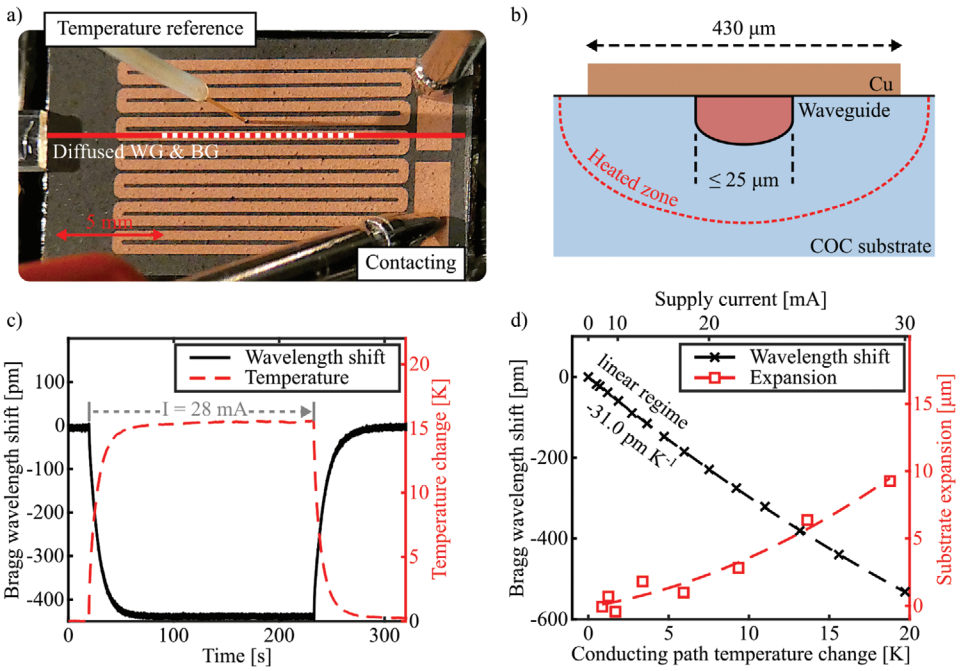

Figure 4. Thermo-optic tuning setup and results. a) Photograph of the electrified COC-PPBG with contacted Cu conducting path and temperature referencing. Additionally, positioning of diffused waveguide (WG) and Bragg grating (BG), located underneath the conducting layer, is indicated. b) Cross-sectional schematic of the employed thermo-optic tuning configuration. c) Time trace of resulting conducting path temperature change and Bragg wavelength shift when applying a current of 28 mA to the Cu structure. d) Bragg wavelength shift and substrate expansion as a function of conducting path temperature or supply current.

temporal temperature evolution. For a supply current of 28 mA, the conducting path's temperature increase saturates at 15 K, which entails a constant maximum Bragg wavelength shift of −439 pm. After discontinuation of the current supply, the Cu structure cools down to room temperature while the Bragg signal returns to its initial value. The maximum Bragg wavelength shift as a function of the conducting path temperature change, induced by various supply currents, is given in Figure 4d. Up to a temperature increase of 9 K, caused by a direct current of 20 mA, the resulting Bragg wavelength shift exhibits a linear behavior whereas linear regression yields a temperature response of −31 pm K^{-1}. The drastic increase of the COC-PPBG's temperature response, in comparison to the thermal referencing experiment, as well as its nonlinear behavior at supply currents beyond 20 mA, can be attributed to the substrate's thermal expansion, also shown in Figure 4d. For small supply currents, there is no or negligible substrate expansion counteracting the negative thermo-optic coefficient of the polymer-based Bragg grating. As indicated by Figure 4b, due to its low thermal conductivity, the heat generated by the Cu path is at first well confined to regions close to the polymer's upper surface. In this case, most of the bulk substrate remains at room temperature which prevents thermal expansion. However, with increasing temperature of the conducting structure, location-dependent expansion or thermal mismatch will result in a deformation of the COC platform, which consequently reduces the responsivity of the thermo-optic structure.

While the overall conducting path exhibits a resistance of 227 Ω at a length of 182 mm, solely the heat generated by the Cu line positioned directly on top of the Bragg grating is responsible for the induced thermo-optic Bragg wavelength shift. Thus, only a conducting-path length of 10 mm has to be taken into account when estimating the actual necessary electric power consumption of the device. The PPBG'S electro-optic tuning efficiency is determined by directly contacting the respective conducting path section, as shown in the inset of **Figure 5**.

Furthermore, Figure 5 depicts the resulting Bragg wavelength shift as a function of the electrical power consumed in the Bragg grating region, acquired by simultaneously monitoring supply current and voltage. The tunable photonic device exhibits a nonlinear dependency toward the supplied electrical power. However, it can be well fitted with a second order polynomial, which is underlined by the obtained R^2 value of 0.9984. While, due to the adapted contacting scheme, the overall substrate expansion is not comparable to earlier observations, there is still local thermal expansion in the Bragg grating region. Thus, this nonlinear behavior is again attributed to local thermal expansion effects in combination with heat convection. The obtained maximum wavelength shift, at an electrical power consumption of 18.3 mW, is determined as −547 pm.

2.4. Spectral Bandwidth Tuning and Versatility

Due to the outstanding flexibility of the employed femtosecond laser-based electrification process, straightforward realization of various conducting path geometries is possible. Thus, the proposed concept of thermo-optic COC-PPBGs can be used in the outline of multiple applications. An exemplary alternative

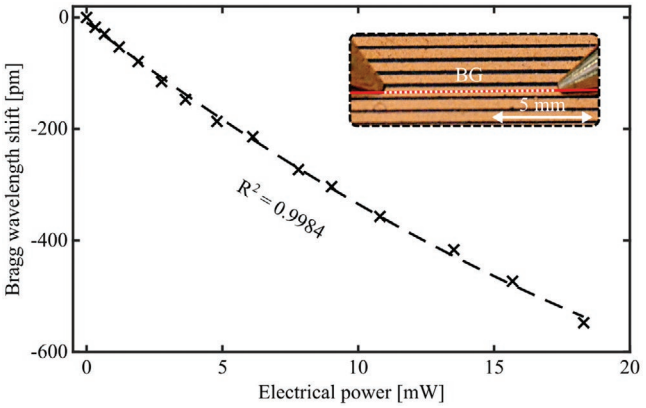

Figure 5. Electrical efficiency. Electrified COC-PPBG's tuning response fitted with a second order polynomial. The inset depicts how the conducting path is contacted in close proximity to the Bragg grating.

to facilitating temperature-induced Bragg wavelength shifts of a PPBG is given in **Figure 6a**.

It shows the FWHM evolution of a partially electrified PPIC, whereas ≈3 mm of a 10 mm long grating is covered with a Cu conducting path exhibiting an overall length of 6 mm and a resistance of 56 Ω. While there is negligible change in the reflection signal of a fully electrified Bragg grating, partial electrification leads to an unambiguous spectral bandwidth increase when exceeding a supply current of 15 mA. Since the grating structure is only partially heated by the Cu conducting path, it can be discretized as two successive uniform Bragg gratings.[49,50] Whereas one structure remains at room temperature and thus exhibits a constant signal, the heated section's reflection peak shifts according to its temperature change. Since the device's overall Bragg peak is a superposition of both partial signals, its spectral width increases. In the examined configuration, a FWHM change of 400 pm correlates to a supply current of 26 mA. Consequently, the demonstrated fabrication method for thermo-optic COC-PPGs enables straightforward adaptation toward multiple applications by adjusting geometry and positioning of the generated Cu structure.

Altogether, an almost limitless variety of 2D structures can be fabricated with this method by changing the beam path of the employed galvanometer scanner, as underlined by the Cu structure depicted in Figure 6b. It features the logo of the "Applied Lasers and Photonics" group (alp), realized as a working Cu conducting path. With an overall length of 35 mm and path widths down to 200 µm, the conducting path features a resistance of 180 Ω, whereas 75% thereof are associated to the meander structure of the "l."

3. Discussion

This contribution demonstrates a novel concept for thermo-optically tunable PPBG devices by combining two advanced fabrication techniques, namely the SWS procedure and FLRS of CuO NPs. The former generates integrated diffused waveguides, comprising an additional Bragg grating structure, within an injection molded COC substrate. Subsequently, electrically conducting Cu paths are generated by FLRS of a CuO precursor layer. In comparison to other state-of-the-art polymer-based thermo-optical devices, the photonic platform is not an elaborate heterostructure, but consists of a bulk polymer slab. This omits the necessity of employing additional silica substrates. Altogether, generation of a thermo-optic COC-PPBG requires only four active production steps whereas devices fabricated with standardized photolithographic procedures need at least twice as many, sometimes up to 16, steps.[12,13,17,51] Additionally, FLRS processes do not require a vacuum atmosphere and thus represent an eco-friendly fabrication method.[52] Moreover, laser-based electrification of the photonic platform offers a high degree of freedom for possible conducting path designs, thus paving the way toward a variety of PPIC applications. The versatility of the proposed method is exemplarily underlined by manufacturing a device that enables controlled adaptation of the reflection signal's spectral width. Additionally, a complex 2D structure with deviating electrical properties is shown. Thus, the proposed fabrication technique is straightforwardly adaptable for alternative applications based on

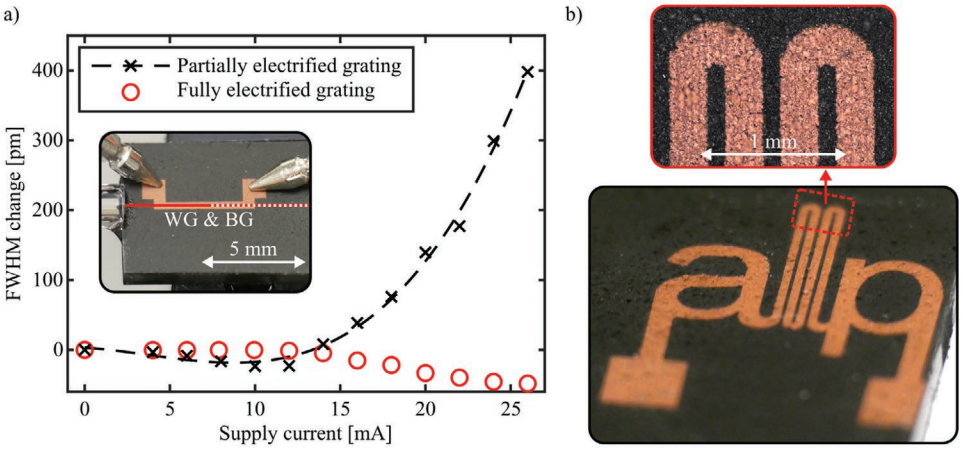

Figure 6. Bandwidth tuning and versatility. a) FWHM tuning of a partially and a fully electrified polymer planar Bragg grating. The inset shows a photograph of a partially electrified grating. b) Exemplary conducting path to underline the versatility of thermo-optic COC-PPBGs manufactured by FLRS of CuO NPs.

thermo-optic tuning of Bragg gratings, such as dispersion compensators, switches, and beam deflectors.[53–55] Furthermore, as already demonstrated by the authors, the employed laser-based technology enables simultaneous generation of microstructures and microfluidic channels, which underlines the device's potential toward biomedical applications or micro-opto-electro-mechanical systems.[41]

After generation of the Cu conducting paths, the fully electrified PPBG exhibits a Bragg wavelength shift of −200 pm and a constant increase in spectral FWHM of 36 pm, whereas these alterations are attributed to local stress fields induced by the copper-to-polymer interconnection or residual local microdamage. Additionally, a temperature referencing cycle on a hotplate reveals a linear temperature sensitivity of −5.1 pm K^{-1} and thus no noticeable deviations compared to untreated COC-PPBGs. Furthermore, the thermal expansion coefficient of the injection-molded COC substrate is determined as $5.62 \cdot 10^{-5}$ K^{-1} by means of a self-built Fabry–Pérot dilatometer. To the author's best knowledge, this is the first thermal expansion quantification of injection molded PPBG substrates manufactured from COC with comparable grade. Since the acquired results correlate well to the specified values of the virgin polymer resin as well as to preliminary temperature experiments on bulk COC-PPBGs and thermo-optic coefficient measurements, the laser-based electrification process has no noticeable impact on the properties of the integrated photonic structures.

Supplying the Cu conducting path with direct current leads to a temperature-induced negative Bragg wavelength shift. Up to a supply current of 20 mA, the reflection signal exhibits a linear response of −31 pm K^{-1} which, compared with heating up the whole device, represents an increased sensitivity by a factor of six. The specimen's behavior can be explained by monitoring and evaluating the polymer substrate's thermal expansion. It is found that there is negligible expansion counteracting the thermo-optic effect at small supply currents. With increasing current, and thus microheater temperature, the polymer platform's elongation increases significantly, which counteracts the tuning response.

The device's electrical efficiency can be well fitted with a second order polynomial. With a Bragg wavelength shift of −547 pm at a consumed electrical power of 18.3 mW, the tunable COC-PPBGs electro-optic efficiency is about two times higher than that of a thermo-optically tunable Bragg grating within a poly(methyl methacrylate) fiber, coated with a Pd/Cu thin film, and that of a silica fiber Bragg grating coated with a Ti/Pt/Ni alloy.[56,57] It is worthwhile to note that the demonstrated devices, especially but not solely the shown Cu conducting path geometries and configurations, are not yet finally optimized for efficient electro-optic tuning. It is therefore expected that the adaptation of various parameters such as conducting path positioning, cross section, and general design yields noticeable further improvement of the electrified COC-PPBG's tuning capabilities. Furthermore, it is possible to force propagation of the guided mode closer to the substrate surface, and therefore the microheater, by adjusting the SWS procedure's irradiation parameters.[23]

While this contribution mainly focuses on using the fabricated device in the outline of electro-thermal tuning of the buried photonic structures, it is also feasible to transfer the concept toward monitoring of integrated electronics since, especially on polymer platforms, temperature control of integrated circuits is crucial.[58] Exemplary applications are the in situ monitoring of microfluidic devices designed for electrophoresis or other photonic micro-electro-mechanical systems.[59–61] Thus, based on the results discussed in this contribution and on behalf of their unambiguous potential, COC-PPBGs electrified with Cu conducting paths, generated by means of FLRS of CuO NPs, constitute a promising concept for future polymer-based electro-optic devices.

4. Experimental Section

Device Fabrication: The photonic platform was generated by employing the SWS procedure. For this purpose, a bulk COC substrate (TOPAS 6017S-04, TOPAS Advanced Polymers, Raunheim, Germany) with a length of 20 mm, a width of 10 mm, and a thickness of 1.1 mm was covered by a phase mask (Ibsen Photonics, Farum, Denmark) and an amplitude mask (Compugraphics Jena, Jena, Germany). The employed phase mask's grating structure had a length of 10 mm and a grating period of 1020 nm while the amplitude mask exhibited a slit width of 27 µm. Subsequently, the polymer was irradiated with an overall UV dosage of 150 J cm^{-2}, generated by a KrF excimer laser (BraggStar Industrial, Coherent, Santa Clara, CA, USA). At a repetition rate of 200 Hz, pulse duration and energy of the employed single pulses were 15 ns and 68 µJ, respectively.

Prior to coating, the polymer's surface was O_2 plasma treated (Pico, Diener electronic, Ebhausen, Germany) at a pressure of 0.2 mbar and a power of 180 W at a frequency of 40 kHz, for a duration of 180 s. Subsequently, the photonic platform was spin coated with a copper(II) oxide NP solution containing 60 wt% NPs with a particle size smaller than 50 nm (ROTInanoMETIC, Carl Roth, Karlsruhe, Germany), 27 wt% ethylene glycol (EG ≥ 99%, Carl Roth) and 13 wt% polyvinylpyrrolidone (K 25, Carl Roth). In dependence on the precursor's viscosity, the rotational speed varied from 3000 to 7,000 rpm so the resulting average coating thickness was 30 µm. Reductive sintering of the CuO NPs was done by means of an ultrashort pulse laser (Pharos-10-600-PP, Light Conversion, Vilnius, Lithuania). The laser radiation, exhibiting a wavelength of 1028 nm, was imaged and positioned on the sample by means of a galvanometer scanner (Rhothor AR800, Newson, Dendermonde, Belgium), equipped with a telecentric f-theta lens with a focal length of 100 mm, which yielded a focal spot size of 38 µm. Positioned at a focal offset of 2 mm, the precursor layer was irradiated with 220 fs laser pulses, exhibiting a pulse energy of 4 µJ and thus a pulse fluence of 80 mJ cm^{-2}, at a repetition frequency of 100 kHz. The scanning speed was optimized toward achieving a constant pulse overlap of 98% within a single track. The final conducting paths consisted of a hatched structure with an overlap of 15% with respect to a single track of the hatch. A comprehensive discussion of the employed process, its parameters, and their impact on the resulting Cu conducting path properties were given by the authors elsewhere.[41]

Evaluation: A commercial-grade interrogation unit (HYPERION si155, Micron Optics, Atlanta, GA, USA) was used to evaluate both, the Bragg reflection of the COC-PPBG and the free spectral range of the Fabry–Pérot dilatometer. By evaluating the first derivative of the boxcar-filtered Bragg reflection spectrum, the device offered spectral resolutions down to 1 pm at measurement rates up to 1 kHz. Additionally, the system was equipped with a depolarization unit to prevent measurement uncertainties due to polarization effects.[62] Quantification of the dilatometer's free spectral range response toward thermal expansion of the measurand was based on mechanical referencing of the interferometer. The process was outlined by means of **Figure 7**.

Before conducting thermal experiments, the distance between fiber and specimen facet was incrementally reduced by means of a linear translation stage. This led to a cavity length dependent change of the

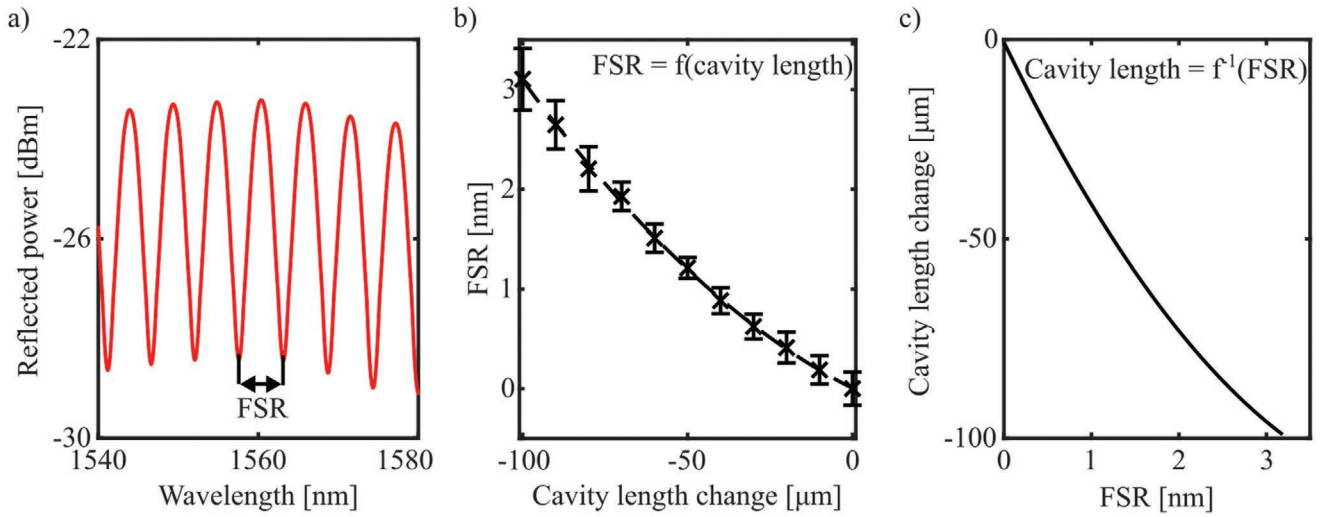

Figure 7. Fabry–Pérot dilatometer referencing procedure. a) Raw interferometric spectrum of the dilatometer whereas the free spectral range (FSR) of the reflection minima is evaluated. b) Evolution of free spectral range acquired by changing the interferometer's cavity length. The error bars represent the one sigma standard deviation of 90 measurements. c) Inverse function used for the quantification of cavity length changes due to thermal expansion processes.

determined FSR. In order to mitigate fluctuations and environmental influences, an average of 90 measurements per sampling point was evaluated to acquire the resulting FSR as a function of the controlled cavity length manipulation. Based on a polynomial fit, the inverse function used to quantify the thermal expansion of a sample was derived. Please note that the referencing procedure needed to be repeated whenever the setup composition was adapted to ensure the validity of the acquired transfer function. Just like during referencing, thermal expansion measurement values were generated out of 90 measurements per sampling point in order to mitigate the influence of thermally induced air fluctuations.

Acknowledgements

Open access funding enabled and organized by Projekt DEAL.

Conflict of Interest

The authors declare no conflict of interest.

Data Availability Statement

The data that support the findings of this study are available from the corresponding author upon reasonable request.

Keywords

Bragg gratings, CuO nanoparticles, cyclic olefin copolymers, electro-optic tuning, integrated photonics, laser reductive sintering

Received: December 18, 2020
Revised: March 10, 2021
Published online: April 7, 2021

[1] G. Ghosh, *Handbook of Optical Constants of Solids: Handbook of Thermo-Optic Coefficients of Optical Materials with Applications*, Academic Press, London **1998**.
[2] Z. Zhang, N. Keil, *Opt. Commun.* **2016**, *362*, 101.
[3] L. Eldada, L. W. Shacklette, *IEEE J. Sel. Top. Quantum Electron.* **2000**, *6*, 54.
[4] H. Ma, A.-Y. Jen, L. R. Dalton, *Adv. Mater.* **2002**, *14*, 1339.
[5] W. H. Wong, K. K. Liu, K. S. Chan, E. Pun, *J. Cryst. Growth* **2006**, *288*, 100.
[6] Z. Zhang, P. Zhao, P. Lin, F. Sun, *Polymer* **2006**, *47*, 4893.
[7] R. Hauffe, K. Petermann, in *Optical Switching* (Ed: T. S. El-Bawab), Springer, Boston, MA **2006**, Ch.4.
[8] K. Kalli, H. L. Dobb, D. J. Webb, K. Carroll, C. Themistos, M. Komodromos, G.-D. Peng, Q. Fang, I. W. Boyd, *Meas. Sci. Technol.* **2007**, *18*, 3155.
[9] U. Siebel, R. Hauffe, J. Bruns, K. Petermann, *IEEE Photonics Technol. Lett.* **2001**, *13*, 957.
[10] Y.-O. Noh, C.-H. Lee, J.-M. Kim, W.-Y. Hwang, Y.-H. Won, H.-J. Lee, S.-G. Han, M.-C. Oh, *Opt. Commun.* **2004**, *242*, 533.
[11] Y.-T. Han, J.-U. Shin, S.-H. Park, S.-P. Han, Y. Baek, C.-H. Lee, Y.-O. Noh, H.-H. Park, *ETRI J.* **2011**, *33*, 275.
[12] Y. Sun, Y. Cao, Q. Wang, Y. Yi, X. Sun, Y. Wu, F. Wang, D. Zhang, *Appl. Opt.* **2018**, *57*, 14.
[13] S.-M. Kim, T.-H. Park, G. Huang, M.-C. Oh, *Polymers* **2018**, *10*, 497.
[14] Y. Gao, Y. Xu, L. Ji, X. Sun, Y. Yi, F. Wang, Y. Wu, D. Zhang, *IEEE Photonics Technol. Lett.* **2019**, *31*, 861.
[15] K.-H. Yoon, B.-S. Choi, O.-K. Kwon, S. H. Oh, K. S. Kim, D. M. Kang, Y.-T. Han, H. K. Lee, *IEEE Photonics Technol. Lett.* **2014**, *26*, 47.
[16] S. H. Oh, K.-H. Yoon, K. S. Kim, J. Kim, O.-K. Kwon, D. K. Oh, Y.-O. Noh, J.-K. Seo, H.-J. Lee, *IEEE J. Sel. Top. Quantum Electron.* **2011**, *17*, 1534.
[17] N.-S. Son, K.-J. Kim, J.-W. Kim, M.-C. Oh, *Opt. Express* **2012**, *20*, 827.
[18] Y.-O. Noh, H.-J. Lee, J. J. Ju, M. Kim, S. H. Oh, M.-C. Oh, *Opt. Express* **2008**, *16*, 18194.
[19] C. Mack, *Fundamental Principles of Optical Lithography: The Science of Microfabrication*, Wiley, Hoboken, NJ **2007**.
[20] M. Rosenberger, G. Koller, S. Belle, B. Schmauss, R. Hellmann, *Opt. Express* **2012**, *20*, 27288.

[21] M. Girschikofsky, M. Rosenberger, M. Förthner, M. Rommel, L. Frey, R. Hellmann, in *Optical Sensing and Detection V*, Proc. SPIE Vol. *10680* (Eds: F. Berghmans, A. G. Mignani), SPIE, Bellingham **2018**, p. 106800P.
[22] M. Rosenberger, S. Hessler, S. Belle, B. Schmauss, R. Hellmann, *Sens. Actuators, A* **2015**, *221*, 148.
[23] M. Rosenberger, B. Schmauss, R. Hellmann, *Opt. Mater. Express* **2016**, *6*, 2118.
[24] S. Hessler, M. Rosenberger, B. Schmauss, R. Hellmann, *Opt. Mater.* **2018**, *75*, 230.
[25] G. Khanarian, *Opt. Eng.* **2001**, *40*, 1024.
[26] M. Rosenberger, S. Kefer, M. Girschikofsky, G.-L. Roth, S. Hessler, S. Belle, B. Schmauss, R. Hellmann, *Opt. Lett.* **2018**, *43*, 3321.
[27] S. Kefer, T. Sauer, S. Hessler, M. Kaloudis, B. Schmauss, R. Hellmann, *Polymers* **2020**, *12*, 715.
[28] S. Kefer, T. Sauer, S. Hessler, M. Kaloudis, R. Hellmann, *Sensors* **2020**, *20*, 5452.
[29] M. Trotter, D. Juric, Z. Bagherian, N. Borst, K. Gläser, T. Meissner, F. von Stetten, A. Zimmermann, *Sensors* **2020**, *20*, 1333.
[30] W. Li, Q. Sun, L. Li, J. Jiu, X.-Y. Liu, M. Kanehara, T. Minari, K. Suganuma, *Appl. Mater. Today* **2020**, *18*, 100451.
[31] B. K. Park, D. Kim, S. Jeong, J. Moon, J. S. Kim, *Thin Solid Films* **2007**, *515*, 7706.
[32] M. S. Cho, W. H. Choi, S. G. Kim, I. H. Kim, Y. Lee, *J. Nanosci. Nanotechnol.* **2010**, *10*, 6888.
[33] M. Mizoshiri, S. Hata, *Res. Rev.: J. Mater. Sci.* **2016**, *4*, 155.
[34] S. Back, B. Kang, *Opt. Lasers Eng.* **2018**, *101*, 78.
[35] J. Lee, B. Lee, S. Jeong, Y. Kim, M. Lee, *Appl. Surf. Sci.* **2014**, *307*, 42.
[36] M. Mizoshiri, K. Aoyama, A. Uetsuki, T. Ohishi, *Micromachines* **2019**, *10*, 401.
[37] H. S. Lee, M. Y. Yang, *Phys. Chem. Chem. Phys.* **2015**, *17*, 4360.
[38] M. Mizoshiri, Y. Kondo, *Jpn. J. Appl. Phys.* **2019**, *58*, SDDF05.
[39] S. Arakane, M. Mizoshiri, J. Sakurai, S. Hata, *J. Micromech. Microeng.* **2017**, *27*, 055013.
[40] S. Arakane, M. Mizoshiri, J. Sakurai, S. Hata, *Appl. Phys. Express* **2017**, *10*, 017201.
[41] G.-L. Roth, J. Haubner, S. Kefer, C. Esen, R. Hellmann, *Opt. Lasers Eng.* **2021**, *137*, 106362.
[42] S. K. Selvaraja, P. Sethi, in *Emerging Waveguide Technology* (Ed: K. Y. You), IntechOpen, London **2018**, Ch.6.
[43] S.-J. Hwang, M.-C. Tseng, J.-R. Shu, H. Her Yu, *Surf. Coat. Technol.* **2008**, *202*, 3669.
[44] S. Roy, C. Y. Yue, Y. C. Lam, Z. Y. Wang, H. Hu, *Sens. Actuators, B* **2010**, *150*, 537.
[45] T. Mizunami, T. V. Djambova, T. Niiho, S. Gupta, *J. Lightwave Technol.* **2000**, *18*, 230.
[46] R. Kashyap, *Fiber Bragg Gratings*, Academic Press, London **2010**.
[47] C. J. Smithells, W. F. Gale, T. C. Totemeier, *Metals Reference Book*, Elsevier Butterworth-Heinemann, Amsterdam **2004**.
[48] TOPAS Advanced Polymers GmbH, TOPAS®COC: Cyclic Olefin Copolymer, https://topas.com/sites/default/files/PRODUCTS-E-28.04.20.pdf (accessed: December 2020).
[49] M. LeBlanc, S. Y. Huang, M. Ohn, R. M. Measures, A. Guemes, A. Othonos, *Opt. Lett.* **1996**, *21*, 1405.
[50] A. D. Kersey, M. A. Davis, H. J. Patrick, M. LeBlanc, K. P. Koo, C. G. Askins, M. A. Putnam, E. J. Friebele, *J. Lightwave Technol.* **1997**, *15*, 1442.
[51] A. M. Al-Hetar, A. B. Mohammad, A. S. M. Supa'at, Z. A. Shamsan, *J. Lightwave Technol.* **2011**, *29*, 171.
[52] B. Kang, S. Han, J. Kim, S. Ko, M. Yang, *J. Phys. Chem. C* **2011**, *115*, 23664.
[53] B. J. Eggleton, J. A. Rogers, P. S. Westbrook, T. A. Strasser, *IEEE Photonics Technol. Lett.* **1999**, *11*, 854.
[54] X. Wu, L. Liu, Y. Zhang, D. Li, W. Wang, L. Xu, *Opt. Commun.* **2006**, *258*, 135.
[55] J.-H. Kim, L. Sun, C.-H. Jang, C. Choi, R. Chen, *Opt. Eng.* **2003**, *42*, 620.
[56] K. Kalli, H. L. Dobb, D. J. Webb, K. Carroll, M. Komodromos, C. Themistos, G. D. Peng, Q. Fang, I. W. Boyd, *Opt. Lett.* **2007**, *32*, 214.
[57] L. Li, J. Geng, L. Zhao, G. Chen, G. Chen, Z. Fang, C. F. Lam, *IEEE Photonics Technol. Lett.* **2003**, *15*, 545.
[58] S. Ogrenci-Memik, *Heat Management in Integrated Circuits: On-Chip and System-Level Monitoring and Cooling*, The Institution of Engineering and Technology, London, UK **2015**, p. 254.
[59] N.-C. Chen, C.-H. Chen, M.-K. Chen, L.-S. Jang, M.-H. Wang, *Sens. Actuators, B* **2014**, *190*, 570.
[60] H. Park, D. Kim, K.-S. Yun, *Sens. Actuators, B* **2010**, *150*, 167.
[61] A.-Q. Liu, X. Zhang, J. Li, S. H. G. Teo, F. L. Lewis, B. Borovic, *Photonic MEMS Devices: Design, Fabrication and Control*, CRC Press, Boca Raton, FL **2009**.
[62] Micron Optics, Inc., Hyperion si155 Optical Sensing Instrument, https://lunainc.com/product/si155-optical-sensing-instrument (accessed: December 2020).